Infrared scattering rate of overdoped $Tl_2Ba_2CuO_{6+\delta}$

Y. C. Ma and N. L. Wang*
Beijing National Laboratory for Condensed Matter Physics, Institute of Physics, Chinese Academy of Sciences, Beijing 100080, People's Republic of China

(Received 29 November 2005; revised manuscript received 13 February 2006; published 3 April 2006)

We present in-plane optical study on $Tl_2Ba_2CuO_{6+\delta}$ single crystals with substantially different T_c. The study reveals that the overdoping does not lead to a further increase of the carrier density but a decrease of scattering rate. The most significant change occurs at low temperature and in the low frequency. A characteristic spectral feature, seen most clearly for the optimally doped sample and commonly ascribed to the mode coupling effect, weakens with doping and disappears in the heavily overdoped sample. Meanwhile, the optical scattering rate evolves from a linear ω dependence to an upward curvature line shape. Both the temperature and frequency dependence of the scattering rate can be described by a power law relation. We elaborate that the overall decrease of the optical scattering rate originates from the increase of both the quasiparticle life time and the Fermi velocity near the $(\pi,0)$ region in the Fermi surface.

DOI: 10.1103/PhysRevB.73.144503 PACS number(s): 74.25.Gz, 74.72.Jt, 74.62.Dh

For high-temperature superconductors (HTSCs) and other strongly correlated electron systems, the scattering rate of carriers contains all relevant information of carrier interactions with other quasiparticles or excitations. Investigating the frequency- and temperature-dependent scattering rates in different regimes in the phase diagram of HTSCs is crucial for understanding the charge behavior and dynamics in cuprate superconductors.[1] In the heavily underdoped regime, a nonmonotonic form of the optical scattering rate $1/\tau(\omega)$ was observed in all crystals with $y<6.5$ in $YBa_2Cu_3O_y$. A two-component model offers a sufficiently accurate interpretation for this behavior.[1,2] As doping level increases up to nearly optimal doping level, a linear frequency-dependent $1/\tau(\omega)$ is commonly observed in the normal state which could be described by a marginal Fermi liquid (MFL) picture, instead of the above two-component approach. Below 700 cm^{-1} there is a sharp depression followed by an overshoot in $1\tau(\omega)$ in the superconducting state. Though not fully understood, this structure has been generally attributed to the interaction of the charge carriers with a bosonic mode.[1,3] With further doping, the cuprates go into the overdoped regime. Recent studies indicate that the overall scattering rate decreases gradually in the normal state. Meanwhile, the above bosonic mode becomes more subtle and almost disappears.[1,3] Whether or not this mode is responsible for the pairing of superconductivity remains a challenging issue.

It is noted that the La-based cuprate (LSCO) could be doped through the whole doping region.[4] However, this system has relatively low superconducting transition temperatures with maximum $T_c\sim30$ K. For Y- or Bi-based families with maximum $T_c\sim90$ K, only limited range in the overdoping side could be achieved in the phase diagram. Extensive experiments have been carried out in the underdoped and optimally doped regimes; comparatively, much less research work has been done in the overdoped, especially in the heavily overdoped region due to the difficulty of making overdoped samples, although there is no complexity from the pseudogap issue. Among the systems with maximum $T_c\sim90$ K, $Tl_2Ba_2CuO_{6+\delta}$ (Tl-2201) is rather exceptional. The system can be synthesized in the whole region of the overdoped side with T_c ranging from 90 K to 0 K.[5,6] In comparison with the Bi-2201 or LSCO, the same overdoping level for Tl-2201 results in much more suppression of T_c. In addition, Tl-2201 has a well-ordered crystal structure with very flat CuO_2 layers far apart from each other, about 11.6 Å, while for Bi-2212, the distance between the two CuO_2 planes in a unit cell is only 3.2 Å, the bilayer splitting will inevitably appear.[7,8] Many complications which could be found in other cuprates such as in Bi-2212 or YBCO were not important here. Therefore, the Tl-2201 system is an ideal candidate for studying the doping-dependent properties in the overdoped side of the cuprate phase diagram. Recently, heat transport,[9] inelastic neutron scattering experiments,[10] polar angular magnetoresistance oscillations (AMRO),[11] and angle resolved photoemission spectroscopy (ARPES)[12] have been done on Tl-2201. Summarizing and analyzing the overall results and discussions from various experiments on Tl-2201 will help us to understand the HTSCs in cuprates.

Among all the powerful tools for studying cuprates, infrared reflectance spectroscopy probes the bulk properties and the electron dynamics as the frequency-dependent dielectric constants can be deduced from the reflectivity, therefore the spectrum of electronic excitations in the energy range characteristic for mobile carriers could be obtained. Furthermore, it would be very helpful to understand the carriers' behaviors in HTSCs if ARPES results were combined with the optical spectroscopy. Very recently, we have successfully grown a series of Tl-2201 single crystals with substantially different T_c. This provides us a good opportunity to investigate the evolution of optical response in the overdoped side. In this study, we concentrate on the charge dynamics as revealed by the optical scattering rate.

Three Tl-2201 single crystals have been selected for optical measurement: one nearly optimal doping with $T_c=89$ K, the second one the mediately overdoped with $T_c=70$ K, and the third the heavily overdoped sample with $T_c=15$ K. The widths of the superconducting transitions are roughly 5 K for all three samples. All the single crystals have shiny planes with good orientations and about 1×1 mm^2

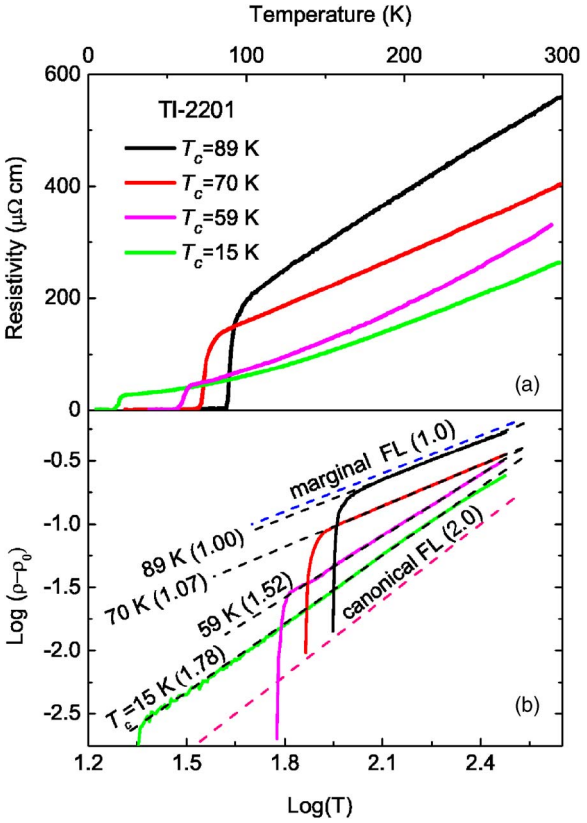

FIG. 1. (Color online) (a) The temperature-dependent resistivity of Tl-2201 single crystals with T_c=89 K, 70 K, 59 K, and 15 K. (b) The log-log plot for Tl-2201 single crystal corresponding to (a). The power law behavior was seen in the whole measured temperature range. The fitting lines with fixed power index were drawn as dashed lines. The model for the MFL and the canonical Fermi liquid are included for comparison.

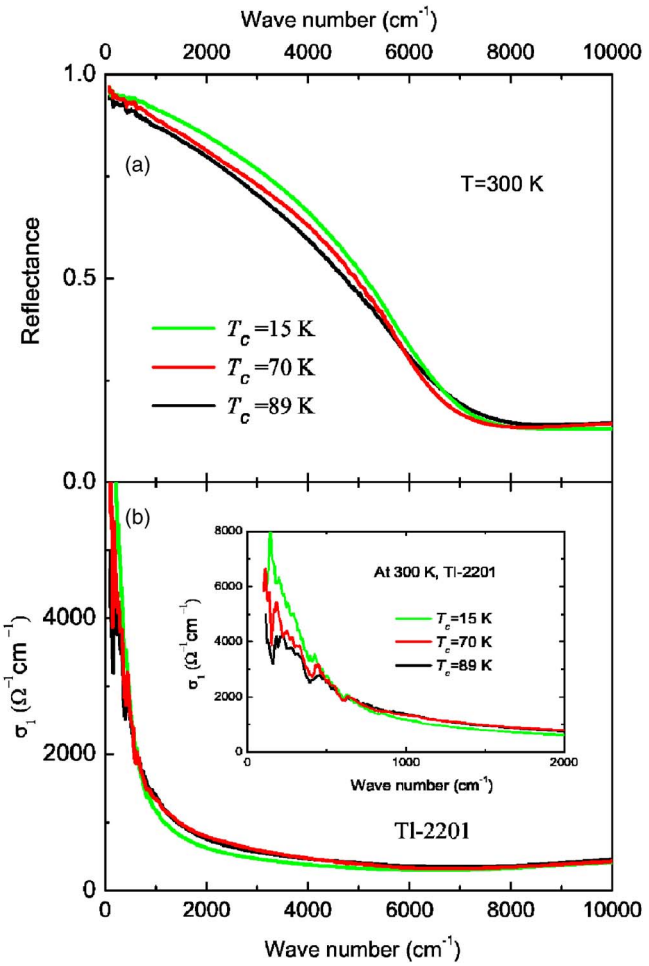

FIG. 2. (Color online) (a) The reflectance data up to 10 000 cm^{-1} at room temperature of three Tl-2201 single crystals with the T_c=89 K, 70 K, and 15 K, respectively. (b) The corresponding conductivity at room temperature calculated from the Kramers-Kronig transformation. Inset: the conductivity spectra in the expanded region at low frequencies.

sizes; the first two samples have been successfully grown by the flux method, see Ref. 13, the third one was also obtained by the same method but with larger oxygen flux. The T_c's of the three samples were characterized by the temperature-dependent dc resistivity. In our experiments, we also measured the dc resistivity of one sample with T_c=59 K, however, due to the small area, it was not appropriate for infrared measurements.

The reflectance measurements from 100 to 22 000 cm^{-1} for $E\|ab$ plane were carried out on a Bruker 66v/S spectrometer. The samples were mounted on optically black cones in a He-gas flowing cryostat with the experimental temperature range 8–320 K and temperature control better than 0.2 K. An *in situ* gold overcoating technique was used for the experiment. The optical conductivity spectra were derived from the Kramers-Kronig transformation. A Hagen-Rubens relation was assumed for the low-frequency extrapolation. At the high-frequency side, a constant extrapolation was adopted up to 100 000 cm^{-1}, then a $R(\omega)\sim\omega^{-4}$ relation was used.

The temperature-dependent dc resistivity $[\rho(T)]$ for Tl-2201 crystals is shown in Fig. 1(a). The resistivity decreases as doping increases in the normal state. The sample with T_c=89 K shows a linear T-dependent resistivity. As the samples become overdoped, a superlinear ρ vs T relation appears. It is found that the T-dependent resistivity actually follows a power-law behavior $\rho(T)\sim T^p$ or, equivalently, in the $\log(\rho-\rho_0)\sim\log(T)$ plot, it displays a linearity behavior, where the slope is the power parameter and ρ_0 is the residual resistivity, as seen in Fig. 1(b). As T_c decreases, the slope or p increases from 1.0 to 1.78. The $\rho(T)$ curves are consistent with the reported data.[5,6]

A comparison of the in-plane optical spectra of three Tl-2201 single crystals at room temperature is shown in Fig. 2. Despite the fairly large decrease in T_c due to the overdoping, the reflectance $R(\omega)$ is found to increase only slightly below roughly 6000 cm^{-1}. This is very different from the spectral evolution in the underdoped side, where the $R(\omega)$ below the reflectance edge changes dramatically with T_c (or doping level).[14] One can estimate the effective carrier number N_{eff} below ω from the conductivity spectral weight (SW) in terms of the partial sum rule:

TABLE I. The spectral weight distribution calculated from Eq. (1) for three Tl-2201 crystals. All the data have been normalized to SW(8000) of the optimally doped sample.

Sample	T_c (K)	SW(600)	SW(8000)-SW(600)	SW(8000)
A	89	0.312	0.688	1.000
B	70	0.367	0.642	1.019
C	15	0.425	0.582	1.007

$$N_{eff}(\omega) = \frac{2mV_{cell}}{\pi e^2}\mathrm{SW}(\omega) = \frac{2mV_{cell}}{\pi e^2}\int_0^{\omega}\sigma_1(\omega')d\omega', \quad (1)$$

where V_{cell} is a unit cell volume. In the optical conductivity spectra shown in Fig. 2(b), only the WS below 600 cm^{-1} increases for samples with lower T_c; the SW between 600 and 8000 cm^{-1} decreases slightly. The overall spectral weight keeps almost constant for the three samples, as seen in Table I. Those results suggest that the effective carrier density does not increase further with doping in the overdoped region, the major change is the narrowing of low-ω Drude-like peak. This narrowing originates from the reduction of the scattering rate, which we shall address below. We note that such characteristic spectral evolution is consistent with an earlier study on Tl-based systems.[15]

Although the overall spectral weight does not change very much, the low-ω $R(\omega)$ at low T changes significantly with overdoping. Figure 3 shows the T-dependent $R(\omega)$ and $\sigma_1(\omega)$ spectra from 100 to 2000 cm^{-1} for the three samples. For the T_c=89 K single crystal, the $R(\omega)$ displays a well-known knee structure near 500 cm^{-1}, followed by a dip at higher

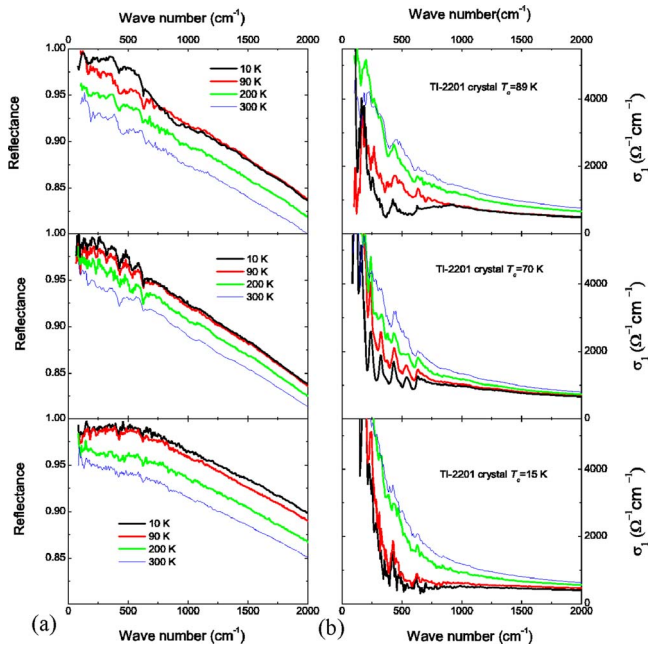

FIG. 3. (Color online) (a) The temperature-dependent reflectance of three Tl-2201 single crystals with the T_c=89 K, 70 K, and 15 K from 100 to 2000 cm^{-1}. (b) The corresponding conductivity spectra extracted from the Kramers-Kronig transformation.

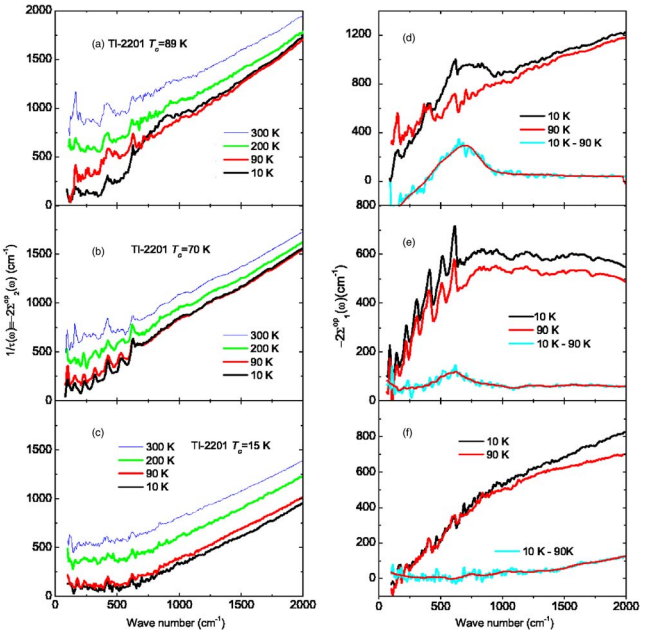

FIG. 4. (Color online) (a)–(c): the doping- and temperature-dependent optical scattering rate $1/\tau(\omega)$ from 100 to 2000 cm^{-1}. (d)–(f): the real part of the optical self-energy of Tl-2201 in the normal state (T=90 K) and superconducting state (T=10 K), as well as the corresponding differences between them. The corresponding smoothed differences have also been shown. (a, d), T_c ~89 K (nearly optimal doped); (b, e), T_c ~70 K (mediately overdoped); (c, f), T_c ~15 K (heavily overdoped).

energy close to 800 cm^{-1} at T=10 K. This feature is commonly observed for cuprate superconductors with high enough T_c. The characteristic structure was usually ascribed to the coupling effect of electrons with a bosonic mode.[1,3,16–22] Since such a line shape causes the depression of low-ω conductivity leading to the missing of some spectral weight, the shape is also related to the superconducting condensate. It is seen clearly that the feature becomes weak as the samples become overdoped and disappears in the heavily overdoped T_c=15 K sample. Note that for the heavily overdoped sample the low-ω $R(\omega)$ is slightly depressed at low temperature, leading to a downward curvature. Such spectral line shape was also observed in earlier studies.[23,24]

A useful way to analyze the carrier dynamics and the mode coupling effect is in terms of the generalized Drude model,[1,3,23]

$$\sigma(\omega) = \frac{i}{4\pi}\frac{\omega_p^2}{\omega - 2\Sigma^{op}(\omega)}, \quad (2)$$

where ω_p is the plasma frequency, which is related to the N_{eff} via the relationship $\omega_p^2 = 4\pi e^2 N_{eff}/mV_{cell} = 8\int_0^{\omega_c}\sigma_1(\omega')d\omega'$ after choosing a proper high-frequency limit ω_c, and Σ^{op} is so-called optical single-partical self-energy: $\Sigma^{OP}(\omega) = \Sigma_1^{OP}(\omega) + i\Sigma_2^{OP}(\omega)$. The imaginary part determines the frequency-dependent carrier scattering rate via $\Sigma_2^{OP}(\omega) \equiv -1/2\tau(\omega))$, while the real part is related to the mass enhancement via $\Sigma_1^{OP}(\omega) \equiv \omega(1-m^*/m)/2$.[3] In Fig. 4, we show

the optical scattering rate as well as the real part of the optical self-energy for the three samples at different temperatures. Here, the plasma frequency $\omega_p = 1.5 \times 10^4$ cm^{-1}, determined by integrating the conductivity up to $\omega_c = 1$ eV, was used for all three samples. We can see that, for the nearly optimally doped sample at 10 K, the scattering rate shows an onset increase near 500 cm^{-1} and an overshoot at frequency corresponding to the dip in the low-T $R(\omega)$. In the real part of the self-energy a sharp peak was seen in the low-T curve. The optical resonance structure was widely attributed to the coupling to a bosonic mode. Clearly, this feature weakens with doping and vanishes for the heavily overdoped sample with $T_c = 15$ K.

Hwang *et al.* studied the self-energy effects in optics for different dopings and temperatures in the Bi-2212 system.[3] They identified that the peak in the real part of the optical self-energy is closely related to the ARPES self-energy obtained by Johnson *et al.* performed at the nodal point.[25] They also found that as the doping level increases, the contribution of the bosonic resonance to the self-energy weakens and disappears in the highly overdoped regime. A similar trend of ARPES self-energy effects with doping near the antinodal point $(\pi, 0)$ was also observed by Kim *et al.* on the Bi-2212 system.[26] However, it should be remarked that both Hwang *et al.* and Kim *et al.* extrapolated their data to a critical doping level of $\delta_c = 0.23-0.24$, where they claimed that the anomalous peak in the real part of the self-energy would no longer exist, but they did not have real data for such doping levels. In our experiments, the corresponding doping level of the $T_c \sim 15$ K overdoped Tl-2201 sample is about $\delta \simeq 0.26$ based on the universal relation between T_c and the doping level for HTSCs.[27] So, it offers an opportunity to clarify the issue. Indeed, the feature caused by the narrow mode is not visible for the heavily overdoped sample. The consistency of the spectral evolution in two different systems suggests that this is the generic property of the Cu-O layers in the overdoped regime of HTSCs.

The nature of the mode involved in the coupling remains under intense debate. Here we remark that the observed spectral feature is not consistent with a coupling with a phonon, but could still be reconciled with a coupling to magnetic excitations. According to neutron scattering experiments, the magnetic resonance mode at (π, π) shows a strong doping dependence: (1) The resonance has the highest energy E_r at the optimal doping, but shifts to lower energy with either increasing or decreasing the doping levels with a preserved $E_r/k_B T_c$ ratio. For Tl-2201, the resonance is seen at $E_r = 47$ meV at optimal doping, and the ratio of $E_r/k_B T_c \simeq 6$.[10,28,29] (2) The spectral weight of the resonance drops sharply in the overdoped regime at the doping level close to $\delta \sim 0.19$.[30] Apparently, in the case of coupling to the magnetic resonance, the coupling feature should also shift to lower frequency and weaken with overdoping. Qualitatively this is indeed what we observed here, as well as the data obtained by Hwang *et al.* for the Bi-2212 system.[3] Additionally, the inhomogeneity, which is inevitably present in those samples, would lead to a further damping of the mode effect. Since neutron experiments were performed only in limited range in the overdoped side, it is not clear whether or not the magnetic resonance mode would disappear in the heavily overdoped sample; then a precise and complete comparison could not be made. Another possibility for the vanishing spectral feature in the heavily overdoped $T_c = 15$ K sample is that the feature shifts to the region below our measurement frequency. It is well known that the characteristic mode-coupling feature in optics should appear at an energy $2\Delta + E_r$,[1,3,16,17] where Δ stands for the maximum of the d-wave superconducting gap. The values of the superconducting gap as a function of hole doping for Tl-2201 are given by Hawthorn *et al.*[31] For $T_c = 15$ K, $2\Delta \sim 5$ meV, while the resonance is expected to appear at $E_r \sim 7.8$ meV based on the above scaling ratio between E_r and T_c,[28,29] then the coupling feature in optics should appear at 100 cm^{-1}. This is already out of the range for getting reliable data on such small size samples in our measurement. Note that, in the case of coupling with a phonon at energy E_p, one can carry out the same discussion, but in such a case, the characristic energy of the phonon should remain almost constant as a function of hole doping: E_p should be about 40–50 meV. The mode coupling effect should be observed around 320–400 cm^{-1}, in the heavily doped sample. That is not consistent with the data presented here.

Besides the vanishing of mode structure, the differential spectra between 10 K and 90 K of the real part of the optical self-energy also show interesting change with doping at high frequencies (800–2000 cm^{-1}). As seen from Figs. 4(d)–4(f), the signal is weak for the nearly optimally doped sample and decreases slightly with increasing energy. The signal increases in the $T_c = 70$ K sample and is almost constant as a function of the energy. It further increases and shifts to higher energy in the $T_c = 15$ K sample. Note that the evolution of the differential spectra is closely related to the forms of the T-dependent reflectance $R(\omega)$, as shown in the left panel of Fig. 3. For the nearly optimally doped sample, $R(\omega)$ is almost temperature independent at high ω below 90 K; however, in the frequency range of 750–1500 cm^{-1}, the reflectance at 10 K is slightly lower than that at 90 K due to the effect of mode coupling or dip structure appearing near 800 cm^{-1}. As the samples become overdoped, the reflectance spectra below 90 K separate from each other gradually. The spectral difference can be naturally ascribed to the different ω- and T-dependent carrier scattering rates for different doping levels. In fact, the real part of optical self-energy is linked with the optical scattering rate (i.e., imaginary part) through the Kramers-Kronig relationship.

We note that, similar to the T-dependent dc resistivity, the ω-dependent behavior of the scattering rate also changes with doping. For the $T_c = 89$ K sample, the $1/\tau(\omega)$ displays a linear-ω dependence in the normal state. As the sample becomes overdoped, the $1/\tau(\omega)$ shows an upward curvature. The behavior is seen very clearly in the heavily overdoped sample with $T_c = 15$ K. As the dc $\rho(T)$ follows a power-law dependence, we expect the same power-law behavior for the ω-dependent scattering rate. Therefore, we suggest that the scattering rate may approximately follow the relation:

$$1/\tau(\omega, T) = 1/\tau_0 + \alpha(k_B T)^p + \beta(\hbar\omega)^p. \quad (3)$$

Here, the first term on the right-hand side is from the impurity scattering, α and β are constants, and p ranges from 1 to

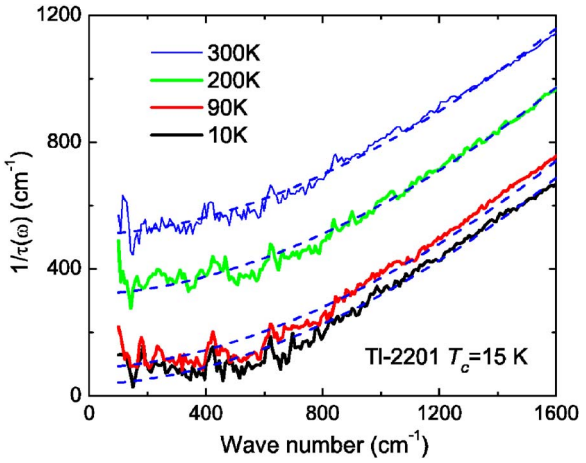

FIG. 5. (Color online) The scattering rates of Tl-2201 with $T_c \sim 15$ K from 100 to 1600 cm^{-1} at different temperatures and the corresponding fittings.

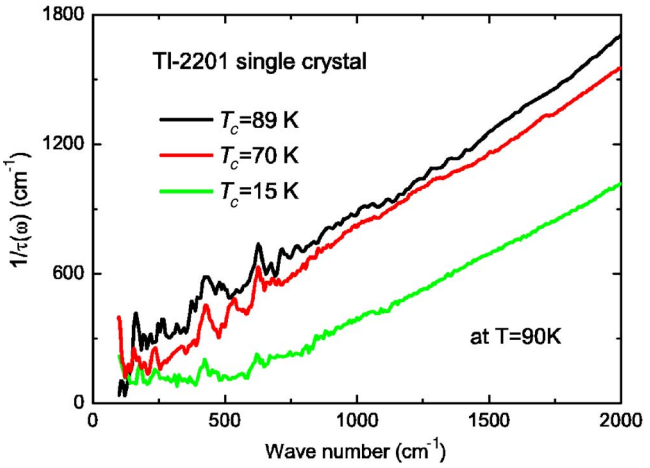

FIG. 6. (Color online) A comparison of the scattering rates for three Tl-2201 single crystals from 100 to 2000 cm^{-1} in the normal state at 90 K.

2. Indeed, we found that this formula successfully describes both T and ω dependence of the scattering rate. Figure 5 shows the $1/\tau(\omega)$ data for the heavily overdoped sample at different temperatures together with fitting curves using the above formula up to 1600 cm^{-1}. Here, we use the value $p=1.78$ determined by the T-dependent dc resistivity in our fitting. We found that $\alpha/\beta \sim (1.6\pi)^2$ best reproduces the $1/\tau(\omega)$ results. Above 1600 cm^{-1}, the $1/\tau(\omega)$ tends to become ω linear dependent, whereas at low ω, a small upturn of $1/\tau(\omega)$ at low T was seen, which corresponds to the unconventional small depression in the reflectance spectrum as mentioned above. This effect is commonly seen for the very overdoped cuprates and addressed in earlier studies.[23,24] It was suggested to be related to the defects in the samples. The fitting results indicate that the $T_c=15$ K sample is still at the intermediate state from MFL to a canonical Fermi-liquid. It should be mentioned that the canonical Fermi liquid behavior ($p=2$) considered here is for the case of the three-dimensional (3D) electron system. For a 2D system, the scattering rate should behave as $1/\tau \sim \alpha T^2 \ln T + \beta\omega^2 \ln \omega$.[32] The fact that both the temperature-dependent dc resistivity and the optical response as a function of frequency follow the trend towards a canonical Fermi liquid fairly well indicates indeed that the system tends to become 3D-like in the overdoped regime, similar to the results obtained from AMRO experiment by Hussey *et al.*[11] This behavior was also consistent with the results of the T-dependent ρ_c/ρ_{ab} in Ref. 33. Nevertheless, the real Fermi liquid state is expected to show up only in non-superconducting samples.

Another remarkable result is that the ω-dependent scattering rate decreases gradually with doping. Implication for this effect was already seen from the Drude component narrowing of the room-temperature conductivity spectra displayed in Fig. 2(b). A careful comparison of the scattering rate spectra indicates that the decrease is present at every measured temperature. As an example, we show in Fig. 6 such a comparison at 90 K for the three samples.

It should be noted that the quasiparticle lifetimes are highly anisotropic around the Fermi surface. The optical scattering rate deduced from the generalized Drude model, Eq. (2), can be taken as an effective average of the scattering rates over Fermi surface, although several comparative studies on ARPES and optical spectroscopy revealed that the optical scattering rate is related more closely to the imaginary part of the self-energy of the quasiparticle near $(\pi/2,\pi/2)$.[3,25,34,35] ARPES experiments revealed that in underdoped curpates, the quasiparticles are sharp near $(\pi/2,\pi/2)$ and ill defined around $(\pi,0)$ in the normal state. Upon increasing doping, the antinodal quasiparticles sharpen up, but they remain broader than the nodal quasiparticles all the way to optimal doping.[36] With further increasing doping in the overdoped side, the antinodal quasiparticles become narrower than the nodal quasiparticles[12] (see the schematic picture of Fig. 7). Those results indicate clearly that the major increase of the quasiparticle lifetime (or reduction of scattering rate) is in the antinodal region. Actually, the recent ARPES study on overdoped Tl-2201 reveals that the nodal quasiparticle peak becomes even broader in heavily overdoped sample than in intermediate overdoped sample.[12] Naively, one can ascribe the reduction of the optical scattering rate when overdoping to the increase of the lifetime of antinodal quasiparticles on the basis of the ARPES results.

However, a more careful consideration suggests that the lifetime increase of the antinodal quasiparticles is not the sole reason for the reduction of the optical scattering rate derived from extended Drude mode: the change of the Fermi velocity arising from the gradual change of the shape of Fermi surface with doping, especially near the antinodal region, also contributes to the transport. Let us elaborate on this point in more detail. According to the generalized Drude model, Eq. (2), the optical scattering rate is derived from the conductivity as $1/\tau(\omega)=(\omega^2/4\pi)\mathrm{Re}(1/\sigma(\omega))$. In the semiclassical approximation, the frequency-dependent conductivity can be expressed as[37]

$$\sigma(\omega) \propto \int \frac{\mathbf{v}_\mathbf{k}^2}{\tau^{-1}(\varepsilon_k) - i\omega}\left(\frac{\delta f}{\delta \varepsilon}\right)_{\varepsilon=\varepsilon_k} d\mathbf{k}/(2\pi)^3, \qquad (4)$$

where $\mathbf{v}_k$ and ε_k are the carrier bare (band-structural) velocity and energy, respectively, $\tau^{-1}(\varepsilon_k)$ is the transport scattering

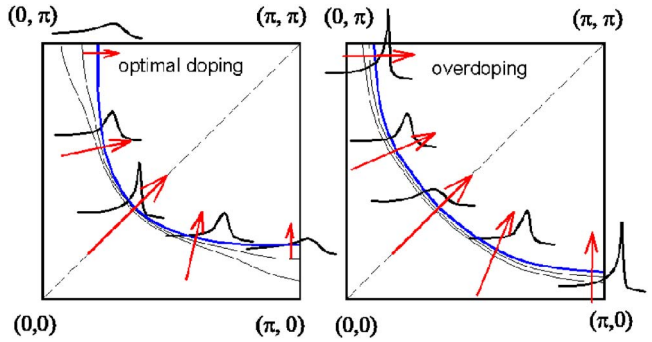

FIG. 7. (Color online) A schematic picture for the Fermi surface, the quasiparticle peak width, and the Fermi velocity at different momentums at the optimal doping (left panel) and overdoping (right panel). The blue curves show the Fermi surfaces, and the gray curves are the equal energy contours. The Fermi velocity (indicated by the red arrow) is the gradient of the Fermi surface, which is apparently large at nodal direction and small near $(\pi,0)$ or $(0,\pi)$. With overdoping, the Fermi velocity increases in the antinodal region. The black curves indicate the quasiparticle peaks as seen in ARPES. The width reflects the inverse of quasiparticle lifetime. For the optimally doped sample, the quasiparticle peak is sharp near the nodal point but broad near $(\pi,0)$ or $(0,\pi)$. In the very overdoped sample, a reversal of the anisotropy is seen.[12]

rate (which is apparently different from the optical scattering rate), and f is the Fermi distribution function. The derivative of f is peaked at the Fermi energy. Actually, this equation was used by Santander-Syro *et al.*[35] to illustrate that the in-plane conductivity was mostly sensitive to the nodal quasiparticles. The integration over all allowed values of $\mathbf{k}$ in Eq. (4) can be transformed into an expression in terms of an integration over the Fermi surface in $\mathbf{k}$-space where the Fermi velocity appears as a weighted factor. The larger the Fermi velocity and the smaller the scattering rate (i.e., the longer quasiparticle lifetime), the larger contribution it has to the transport. For underdoped or even optimally doped cuprates, the Fermi surface has curvature near $(\pi/2,\pi/2)$ but flat near $(\pi,0)$ or $(0,\pi)$, as shown in the left panel of Fig. 7. Then, the gradient of the Fermi surface, which gives the Fermi velocity $\mathbf{v}_k=(1/\hbar)\nabla_{\mathbf{k}}\varepsilon(\mathbf{k})$, is highly anisotropic. Based on the equal energy contours shown as the schematic picture in Fig. 7,[38] the momentum change for the same energy interval in the direction perpendicular to the Fermi surface is larger near $(\pi,0)$ or $(0,\pi)$ than near $(\pi/2,\pi/2)$. This means smaller Fermi velocity near $(\pi,0)$ or $(0,\pi)$ than near $(\pi/2,\pi/2)$. As a result, the in-plane transport is governed by the quasiparticles in the nodal region. However, for the overdoped cuprates, the Fermi surface becomes more circlelike (see the right panel of Fig. 7), the anisotropy of $\mathbf{v}_k$ resulting from the Fermi surface gradient becomes much smaller, then the contribution from the quasiparticles in the antinodal region will increase. To summarize, both the increase of the Fermi velocity and the reduction of carrier scattering near the antinodal region contribute to the in-plane conductivity and, as a result, lead to the reduction of the in-plane optical scattering rate as defined from the generalized Drude model.

In summary, infrared studies of Tl-2201 single crystals for three various doping levels have been carried out. Different from the spectral evolution in the underdoped side, the overall spectral weight does not increase further with doping in the overdoped side; the major change is the narrowing of the Drude-like component due to the reduction of the carrier scattering rate. On the other hand, the low-temperature and low-frequency spectra show significant change with doping. A clear knee structure followed by a dip at higher frequency in the reflectance was observed for a sample close to the optimal doping. Correspondingly, an onset increase followed by an overshoot could be seen in optical scattering rate spectra. Those features, which were commonly ascribed to the mode coupling effect, weaken with doping and vanish for the heavily overdoped sample. We point out that this is a generic property for the cuprates in the overdoped side. Furthermore, we found that the optical scattering rate evolves from a linear ω dependence near optimal doping to a shape with upward curvature upon further doping. Both the temperature and frequency dependence of the scattering rate can be described by a power law relation. We also elaborate that the overall decrease of the optical scattering rate originates from the increase of both the quasiparticle lifetime and the Fermi velocity near the $(\pi,0)$ region in the Fermi surface.

ACKNOWLEDGMENTS

This work was supported by the Ministry of Science and Technology of China (973 Project No. 2006CB601002), the National Science Foundation of China, and the Knowledge Innovation Project of Chinese Academy of Sciences.

*E-mail address: nlwang@aphy.iphy.ac.cn

[1] D. N. Basov and T. Timusk, Rev. Mod. Phys. **77**, 721 (2005).
[2] Y. S. Lee, K. Segawa, Z. Q. Li, W. J. Padilla, M. Dumm, S. V. Dordevic, C. C. Homes, Y. Ando, and D. N. Basov, Phys. Rev. B **72**, 054529 (2005).
[3] J. Hwang, T. Timusk, and G. D. Gu, Nature (London) **427**, 714 (2004).
[4] S. Uchida, T. Ido, H. Takagi, T. Arima, Y. Tokura, and S. Tajima, Phys. Rev. B **43**, 7942 (1991).
[5] Y. Kubo, Y. Shimakawa, T. Manako, T. Satoh, S. Iijima, T. Ichihashi, and H. Igarashi, Physica C **162-164**, 991 (1989).
[6] Y. Shimakawa, Y. Kubo, T. Manako, and H. Igarashi, Phys. Rev. B **40**, R11400 (1989).
[7] A. D. Gromko, A. V. Fedorov, Y.-D. Chuang, J. D. Koralek, Y. Aiura, Y. Yamaguchi, K. Oka, Y. Ando, and D. S. Dessau, Phys. Rev. B **68**, 174520 (2003).
[8] D. L. Feng, N. P. Armitage, D. H. Lu, A. Damascelli, J. P. Hu, P. Bogdanov, A. Lanzara, F. Ronning, K. M. Shen, H. Eisaki, C. Kim, J.-i. Shimoyama, K. Kishio, and Z.-X. Shen, Phys. Rev. Lett. **86**, 5550 (2001).

[9] C. Proust, E. Boaknin, R. W. Hill, L. Taillefer, and A. P. Mackenzie, Phys. Rev. Lett. **89**, 147003 (2002).
[10] H. He, P. Bourges, Y. Sidis, C. Ulrich, L. P. Regnault, S. Pailhes, N. S. Berzigiarova, N. N. Kolesnikov, and B. Keimer, Science **295**, 1045 (2002).
[11] N. E. Hussey, M. Abdel-Jawad, A. Carrington, A. P. Mackenzie, and L. Balicas, Nature (London) **425**, 814 (2003).
[12] M. Platé, J. D. F. Mottershead, I. S. Elfimov, D. C. Peets, R. Liang, D. A. Bonn, W. N. Hardy, S. Chiuzbaian, M. Falub, M. Shi, L. Patthey, and A. Damascelli, Phys. Rev. Lett. **95**, 077001 (2005).
[13] Y. C. Ma and N. L. Wang, Phys. Rev. B **72**, 104518 (2005).
[14] N. L. Wang, A. W. McConnell, and B. P. Clayman, Phys. Rev. B **60**, 14883 (1999).
[15] A. V. Puchkov, P. Fournier, T. Timusk, and N. N. Kolesnikov, Phys. Rev. Lett. **77**, 1853 (1996).
[16] J. P. Carbotte, E. Schachinger, and D. N. Bosov, Nature (London) **401**, 354 (1999).
[17] A. Abanov, A. V. Chubukov, and J. Schmalian, Phys. Rev. B **63**, 180510(R) (2001).
[18] N. L. Wang, T. Timusk, J. P. Franck, P. Schweiss, M. Braden, and A. Erb, Phys. Rev. Lett. **89**, 087003 (2002).
[19] J. J. Tu, C. C. Homes, G. D. Gu, D. N. Basov, and M. Strongin, Phys. Rev. B **66**, 144514 (2002).
[20] N. L. Wang, P. Zheng, J. L. Luo, Z. J. Chen, S. L. Yan, L. Fang, and Y. C. Ma, Phys. Rev. B **68**, 054516 (2003).
[21] S. V. Dordevic, C. C. Homes, J. J. Tu, T. Valla, M. Strongin, P. D. Johnson, G. D. Gu, and D. N. Basov, Phys. Rev. B **71**, 104529 (2005).
[22] J. Hwang, J. Yang, T. Timusk, S. G. Sharapov, J. P. Carbotte, D. A. Bonn, R. Liang, and W. N. Hardy, Phys. Rev. B **73**, 014508 (2006).
[23] A. V. Puchkov, D. N. Basov, and T. Timusk, J. Phys.: Condens. Matter **8**, 10049 (1996).
[24] A. V. Puchkov, T. Timusk, S. Doyle, and A. M. Hermann, Phys. Rev. B **51**, R3312 (1995).
[25] P. D. Johnson, T. Valla, A. V. Fedorov, Z. Yusof, B. O. Wells, Q. Li, A. R. Moodenbaugh, G. D. Gu, N. Koshizuka, C. Kendziora, S. Jian, and D. G. Hinks, Phys. Rev. Lett. **87**, 177007 (2001).
[26] T. K. Kim, A. A. Kordyuk,S. V. Borisenko, A. Koitzch, M. Knupfer, H. Berger, and J. Fink, Phys. Rev. Lett. **91**, 167002 (2003).
[27] M. R. Presland, J. L. Tallon, R. G. Buckley, R. S. Liu, and N. E. Flower, Physica C **176**, 95 (1991).
[28] Y. Sidis, S. Pailhes, B. Keimer, P. Bourges, C. Ulrich, and L. P. Regnault, Phys. Status Solidi B **241**, 1204 (2004).
[29] P. Bourges, B. Keimer, S. Pailhes, L. P. Regnault, Y. Sidis, and C. Ulrich, Physica C **424**, 45 (2005).
[30] S. Pailhes, C. Ulrich, B. Fauque, V. Hinkov, Y. Sidis, A. Ivanov, C. T. Lin, B. Keimer, and P. Bourges, cond-mat/0512634 (unpublished).
[31] D. G. Hawthorn, S. Y. Li, M. Sutherland, E. Boaknin, R. W. Hill, C. Proust, F. Ronning, M. A. Tanatar, J. Paglione, D. Peets, R. Liang, D. A. Bonn, W. N. Hardy, N. N. Kolesnikov, and L. Taillefer, cond-mat/0502273 (unpublished).
[32] L. Zheng and S. Das Sarma, Phys. Rev. B **53**, 9964 (1996).
[33] A. M. Hermann, H. M. Duan, W. Kiehl, and M. Paranthaman, Physica C **209**, 199 (1993).
[34] D. N. Basov, C. C. Homes, E. J. Singley, M. Strongin, T. Timusk, G. Blumberg, and D. van der Marel, Phys. Rev. B **63**, 134514 (2001).
[35] A. F. Santander-Syro, R. P. S. M. Lobo, N. Bontemps, Z. Konstantinovic, Z. Z. Li, and H. Raffy, Phys. Rev. Lett. **88**, 097005 (2002).
[36] A. Damascelli, Z. Hussain, and Z.-X. Shen, Rev. Mod. Phys. **75**, 473 (2003).
[37] N. W. Ashcroft and N. D. Mermin, *Solid State Physics* (Saunders College, Philadelphia, 1976), p. 252.
[38] M. Eschrig and M. R. Norman, Phys. Rev. B **67**, 144503 (2003).